Version 8

Structural Inhomogeneities in $FeTe_{0.6}Se_{0.4}$: Relation to Superconductivity

K. Prokeš,[1,*] M. Schulze,[2] S. Hartwig,[1] N. Schäfer,[1] S. Landsgesell,[1] C.G.F. Blum,[2] D. Abou-Ras,[1] M. Y. Hacisalihoglu,[2,3] E. Ressouche,[4] B. Ouladdiaf,[5] C. Hess,[2] B. Büchner,[2,6] and S. Wurmehl[2,6,†]

[1] *Helmholtz-Zentrum Berlin für Materialien und Energie, Hahn-Meitner Platz 1, D-14109 Berlin, Germany*
[2] *Leibniz-Institut für Festkörper- und Werkstoffforschung (IFW) Dresden, D-01069 Dresden, Germany*
[3] *Karadeniz Technical University, Department of Physics, 61080 Trabzon, Turkey*
[4] *SPSMS, UMR-E CEA/UJF-Grenoble 1, INAC, Grenoble, F-38054, France*
[5] *Institut Laue-Langevin, F-38042 Grenoble Cedex, France*
[6] *Institut für Festkörperphysik, Technische Universität Dresden, Dresden, Germany*

(Dated: December 4, 2014)

Chemical and structural phase compositions of two single-crystalline samples prepared with different cooling rates from stoichiometric $FeTe_{0.6}Se_{0.4}$ melts were studied. Both types of samples were investigated in a very comprehensive way using magnetic and electrical transport measurements combined with X-ray, neutron and electron backscatter diffraction. We show that slowly cooled samples are homogeneous on a microscopic scale with only a slight excess of iron. However, they do not exhibit bulk superconductivity down to 1.8 K. In contrast, fast-cooled samples are superconducting below about 14 K but are composed of several chemical phases: They consist of a matrix preserving the crystal structure of slow-cooled samples, and of core-shell structured dendritic inclusions (about 20-30 vol.%). These have different crystal structure and chemical composition and order magnetically at temperatures far above the superconducting transition temperature of the inhomogeneous samples. We conclude that structural and chemical inhomogeneities that were reported also by other groups are not just unimportant impurities. They play a vital role in the superconducting mechanism of this and similar iron-based systems as they lead to internal stress and act in a similar way as the application of the external pressure that reportedly increase the superconducting transition temperature in many iron pnictides and chalcogenides. We argue that a phase pure, homogeneous and stress-free $FeTe_{0.6}Se_{0.4}$ is non-superconducting.

PACS numbers: x.xx.xx

To investigate the correlation between magnetism and superconductivity (SC) in general, materials are currently under investigation in which both phenomena coexist and in which their coexistence can be tuned by some external parameter. The iron chalcogenides $Fe_{1+y}Te_{1-x}Se_x$ that belong to this class of systems may be considered structurally the simplest of the Fe-based superconductors (space group $P4/nmm$ (No. 129), with room-temperature lattice parameters of $a = b \approx 3.8$ Å, $c \approx 6.1$ Å)[1–5]; they are reported to be grown in the form of large crystals and offer the possibility to tune superconducting/magnetic properties by substitution of Se for Te[6–8] and by application of pressure[9,10].

Stoichiometric FeTe exhibits antiferromagnetic (AFM) order below $T_N = 65$ K with traces of a SC phase below $T_c = 8$ K[11,12]. It has been claimed that superconductivity exists in $Fe_{1+y}Te_{1-x}Se_x$ for all Se doping levels[13] with AFM order extending up to $x = 0.18$[14]. However, other studies showed that Se on Te sites suppresses the magnetic ordering already at around $x = 0.09$ with bulk superconductivity existing for $x \geq 0.29$[6]. Some studies showed that incommensurate magnetic order and superconductivity for a certain Se concentrations coexist[15,16]. Both, superconducting and magnetic properties are known to critically depend on the iron excess[16–20]. The element Fe occupies two different crystallographic positions: position 2*a* at (3/4 1/4 0) denoted as a Fe1 position and position 2*c* at (1/4 1/4 z) with z $\approx$ 0.70, denoted as Fe2. Iron atoms in the former position build square-planar sheets that are usually fully occupied. Atoms in the Fe2 position are at interstitial sites between Te/Se atoms. While the former iron atoms are itinerant, Fe2 type atoms are localized with a magnetic moment of $\approx 2.5\ \mu_B$[18,21] and are destructive for the superconductivity. The treshold is dependent on the concentration of Se in the system and is in the range of very few at. %[16].

The superconducting transition temperature T_c can be raised up to 14 K for a composition of around $x = 0.40$ with Fe2 keeping below 2-3 %. Many controversial reports concerning the mutual coexistence/interplay of AFM and SC exist in literature[9] which may be, at least in part, related to different preparation methods. Influence of annealing[22–24] and different contents of iron[16–20] have been studied intensively, however, very little attention has been given to the influence of cooling rates[25]. Although the majority of the studies[22,26]) suggest, that the prepared polycrystalline or single-crystalline $Fe_{1+y}Te_{1-x}Se_x$ samples contain, depending on preparation conditions, secondary phases (mostly Fe_7Se_8, Fe_3Se_4 or Fe_3O_4), a study dedicated to clarify whether these phases are just unwanted complication or

whether they may play a key role in superconductivity of this system is, so far, missing. In particular, chemical phase segregation has been mentioned in the literature on $Fe_{1+y}Te_{1-x}Se_x$ polycrystals[13,27] as well as single crystals[7,28,29]. Moreover, apart from work dealing with sample characterization, more sophisticated studies on the local structure using x-ray absorption fine structure are consistent with such a segregation[30,31]. Unfortunately, as stated above, the relation between preparation conditions, potential chemical phase segregation, and their impact on superconductivity in this system has not yet been carefully worked out.

In the present contribution, we report a study performed on two kinds of single crystals with a nominal $FeTe_{0.6}Se_{0.4}$ composition exposed to different cooling treatments during growth combining microscopic (X-ray and neutron diffraction, electron microscopy) and macroscopic (electrical resistivity, magnetic susceptibility and magnetization) measurement techniques. We show that one single crystal that appears to be homogeneous without a significant excess of interstitial Fe2 and without variation in the composition is non-superconducting. A perhaps even more remarkable result of our study is that the second crystal that contains macroscopically large inclusions of a secondary phase that are apparently magnetically ordered at low temperatures does show superconductivity. These results manifest that the chemical phase segregation (or consequences of that) is actually a necessary condition for the occurence of superconductivity in $Fe_{1+y}Te_{1-x}Se_x$.

I. EXPERIMENTAL DETAILS

All growth experiments have been carried out using metallic iron (Fe pieces, 99.7%), tellurium (Te pieces, 99.999%) and selenium (Se shots, 99.999%). Pieces of Fe were additionally cleaned with citric acid, rinsed with distilled water and ethanol, then dried under vacuum. Clean Te was obtained from larger Te ingots, which were broken into smaller pieces in an agate mortar. Only pieces with a shiny surface were selected for the subsequent growth experiments. Se shots were used without further cleaning. All materials for sample preparation were stored and handled in a argon-glove box. Crystals with nominal $FeTe_{0.6}Se_{0.4}$ composition were grown from the melt using stoichiometric amounts of the elements by applying a modified Bridgman method. The total amount of 12 g of starting material was sealed in ampoules filled with 0.3 bar argon gas. The growth experiments were carried out within a horizontal two-zone furnace under constant argon flow. At the beginning of the experiments, both temperature zones were heated with the same rate of 5 $Kmin^{-1}$ to 923 K and held for twelve hours to allow for pre-reacting of the elements, followed by heating with 5 $Kmin^{-1}$ to 1133 K. A dwell time of 24 h was used to ensure a homogeneous melt. Afterwards, one zone of the furnace was cooled down by 15 K to establish a temperature gradient. The temperature was held for one hour to stabilize this temperature profile. Subsequently, both zones were cooled down simultaneously. Upon reaching 943 K, the samples were furnace-cooled to ambient temperature.

Two types of samples were obtained, depending on the cooling rate: one which was cooled with cooling rate 2 °C/h (in the following referred to as SC sample) and one which was cooled down slowly with cooling rate of 0.2 °C/h (denoted as NSC sample). Both samples investigated in this study were taken from the middle part of the ingot, exhibit smooth, shiny and metallic-like surfaces by looking at them with the naked eye and both types of samples can be cleaved along the *ab* plane.

The phase purity and crystal structure was studied by X-ray powder diffraction on powders made from crystals using a STOE STADI diffractometer in transmission with Mo-K_{α_1} radiation equipped with a Germanium monochromator and a DECTRIS MYTHEN 1K detector. The surface morphology and chemical composition of both crystals were examined by scanning electron microscopy (SEM). The examined sample fractions were freshly cleaved, in some cases polished, attached to a sample holder, transferred to the microscope in an air sealed compartment and directly inserted into the vented highvacuum chamber of the SEM. The exposure time to air was limited to a minimum, being of the order of very few minutes.

Analyses by scanning electron microscopy were performed on freshly cleaved and polished single crystals, since the material surface quality deteriorates significantly with time exposed to air. Two microscopes were used: a Philips XL30 equipped with an microprobe analyzer (energy-dispersive X-ray spectrometry, EDX) for semiquantitative elemental analysis, and a Zeiss UltraPlus with a combined electron backscatter diffraction (EBSD) and EDX measurement system (Oxford Instruments AZtec, using NordlysNano EBSD and 80mm^2 X-Max X-ray detectors). The acceleration voltage applied was 15 kV.

The temperature dependence of the static magnetic susceptibility χ=M/H, where M and H denote the applied magnetic field and magnetization were measured in the temperature range between 1.8 and 350 K and in fields of up to 14 T on single crystals used for SEM by use of a Quantum Design physical property measurement system (PPMS) model 6000 and a *DC* vibrating sample magnetometer (VSM) Option module. Additional measurements, especially with emphasis on the low-field range were performed using a *Quantum Design* MPMS-XL SQUID magnetometer. In this case, temperature dependent magnetization was measured in the range of 2 to 50 K in a field of 20 Oe under zero-field-cooled (zfc) and field-cooled (fc) conditions.

Neutron diffraction experiments were performed on the CYCLOPS and D23 diffractometers at the Institut Laue Langevin using a standard cryostats capable of reaching temperatures down to 1.7 K. The recently

constructed CYCLOPS is a Laue-technique neutron instrument that uses an array of CCD cameras and a large range of incident neutron wavelengths. It was used to check the crystallinity of both samples. The D23 diffractometer is equipped with a conventional ^{3}He single detector providing a high detection efficiency of diffracted intensities of individually recorded Bragg reflections. To determine the structural details of the homogeneous NSC sample, 196 nuclear reflections were collected on D23 at 1.7 K using incident neutron wavelength of λ=1.279 Å. The platelet-like samples wrapped in an aluminium foil (to avoid thermal stress) which was attached to an aluminium holder with its c-axis perpendicular to the rotational axis of both diffractometers.

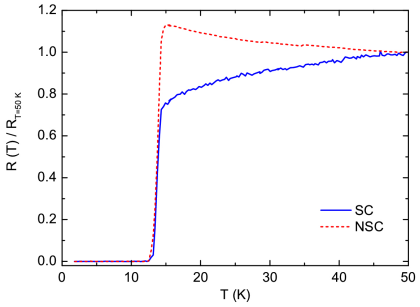

FIG. 1: (Color online) The temperature dependence of the relative electrical resistance of the SC (inhomogeneous) and NSC (homogeneous) samples measured in zero field with current within the $a-b$ plane, normalized to the corresponding 50 K values.

II. RESULTS

A. Bulk measurements

In Fig. 1, we show the temperature dependence of the electrical resistances of the SC and NSC samples measured upon cooling in zero field with current within the $a-b$ plane in the temperature range from 50 - 5 K. We show relative values, normalized to the corresponding values at 50 K. Both samples show a significant drop in the resistance with mid-point at 13.7 K, marking the SC phase transition temperature. The SC sample reaches a negligible resistance below 13 K, the NSC one at 12.8 K. However, the shape of both curves is very different at higher temperatures in the normal state. While the NSC sample resembles with its increasing resistance on cooling the semiconducting-like type resistance of FeTe (see Fig. 5 in Ref.[5]) , the SC sample behaves as a typical metal and follows temperature dependence typical for FeSe[5]. Similarly different temperature slopes were observed in $Fe_{1+y}Te_{1-x}Se_x$ single crystals (x ≈ 0.45-0.48) for different iron contents of 1.09 and 1.04, respectively (see Fig. 2 in Ref.[17]).

Fig. 2(a) shows the volume susceptibility of the inhomogeneous SC sample as function of temperature measured under field cooled (fc) and zero field cooled (zfc) conditions with the magnetic field (20 Oe) aligned along the $a-b$ plane. The two fc and zfc curves magnetization clearly split at 13 K, with the zfc curve exhibiting an appreciable diamagnetic signal, indicating a SC ground state for this sample. The zfc susceptibility data are consistent with the Meissner-type diamagnetic response measured at 2 K as function of low magnetic field (see inset of Fig. 2). Please note, that this clear superconducting transition and the corresponding temperature is typical for all samples which were fastly cooled down and consistent with literature (compare e.g.[5,22]). The volume fraction of the superconducting phase on the SC sample seems to be even larger than 100 % (see Fig. 2(a)). However, since the magnetization has been measured on

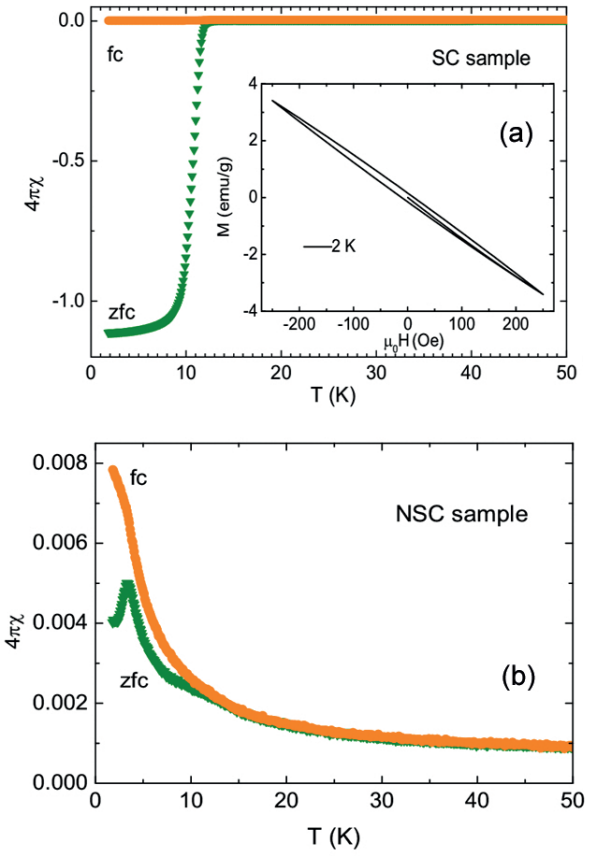

FIG. 2: (Color online) (a) The temperature dependence of the volume magnetic susceptibility of the inhomogeneous SC sample measured under field cooled (fc) and zero field cooled (zfc) conditions with the magnetic field (20 Oe) aligned along the $a-b$ plane. The pure diamagnetic signal measured at 2 K as function of field is shown in the inset. (b) The temperature dependence of the volume magnetic susceptibility of the homogeneous NSC sample measured under field cooled (fc) and zero field cooled (zfc) conditions with the magnetic field (20 Oe) aligned along the $a-b$ plane.

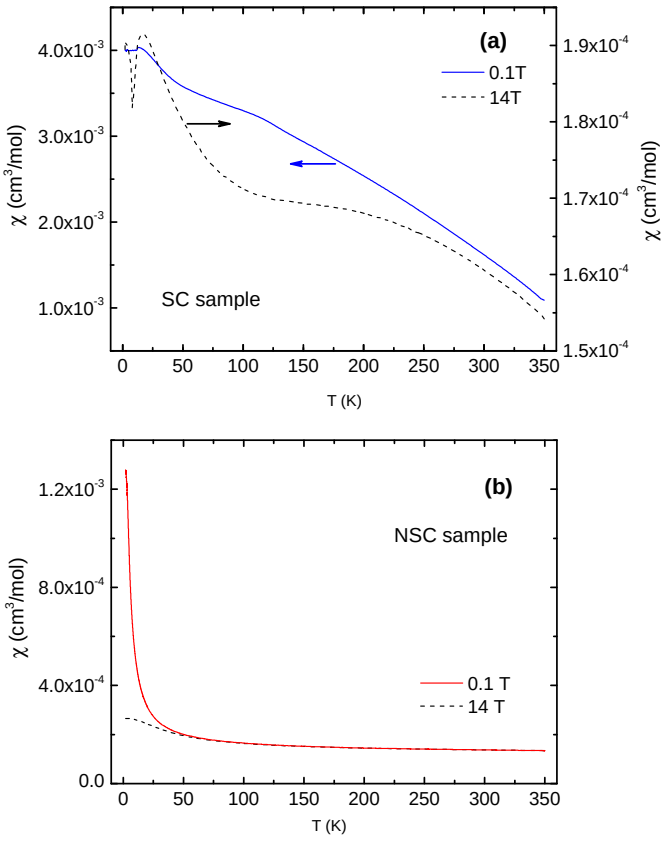

FIG. 3: (Color online) (a) The temperature dependence of the volume magnetic susceptibility of the inhomogeneous SC sample measured with field of 0.1 and 14 T applied within the $a-b$ plane upon cooling. (b) The temperature dependence of the volume magnetic susceptibility of the homogeneous NSC sample measured with field of 0.1 and 14 T applied within the $a-b$ plane upon cooling.

a large single crystal, shielding phenomena are at play that may substantially modify this value. Moreover, as we show below, the magnetization consists (due to inhomogeneous nature of the sample) from at least two major contributions - one originating from the matrix and the other caused by magnetic secondary phase.

In Fig. 3(a) we show the temperature dependence of the volume magnetic susceptibility of the inhomogeneous SC sample measured with field of 0.1 and 14 T applied within the $a-b$ plane upon cooling. As can be seen, the magnetic susceptibility evaluated as $\chi = M/H$ for neither of the applied fields follows Curie-Weiss-like behavior. Such a dependence is reported rather commonly for this system in the literature[5,10,17] and is taken as a hint for low content of the interstitial Fe2 atoms. Room temperature magnetic susceptibility measured at 0.1 T amounts to 1.6x10^{-3}cm^3/mol, a value that suggests 2-

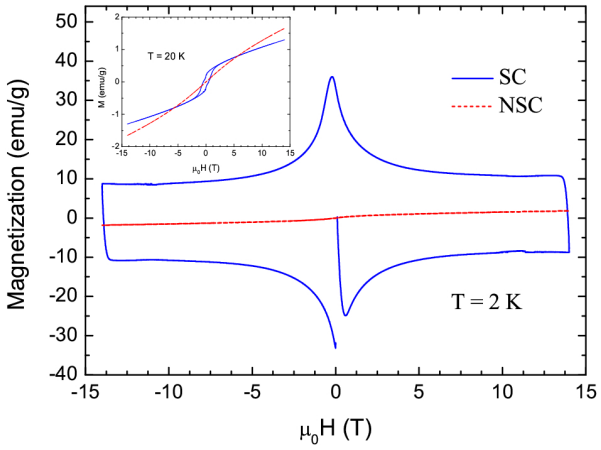

FIG. 4: (Color online) The magnetic field dependence of the magnetization curves at 2 K measured on zero-field cooled SC and NSC samples. In the inset curves taken on both samples at 20 K are shown

3 % of Fe2 being in our sample[5,19,22]. The susceptibility nevertheless increases upon cooling, attains a maximum around 14 K and drops with further lowering the temperature where it eventually saturates. The susceptibility measured at 14 T on cooling shows much lower values suggesting that the susceptibility changes as a function of the applied field. At low temperatures we observe that the susceptibility exhibits a maximum at 16 K, followed by a steep decrease, reaches local minimum at 8 K and increases with further temperature decrease. Noteworthy is a broad "knee" visible at both fields at higher temperatures. In field of 0.1 T it is located around $\approx$ 120 K. It broadens very much and shifts to $\approx$ 240 K at 14 T.

Fig. 3 (b) shows the temperature dependences of the volume magnetic susceptibility of the homogeneous NSC sample measured in the same configuration with identical fields as in the case of the SC sample. The magnetic susceptibility measured at 0.1 T at room temperature is very low (1.4x10^{-4}cm^3/mol) suggesting a negligible amount of Fe2. The susceptibility measured at 14 T gives at room temperature the same value. However, with lowering temperature the two susceptibilities start to deviate, the one measured at 0.1 T being significantly larger below $\approx$ 80 K. Clearly, the susceptibility of this sample exhibits a modified Curie-Weiss (MCW) behavior $\chi = \chi_0 + C/(T-\theta)$ at both fields, where C denotes the Curie constant, θ the Weiss temperature and χ_0 is the temperature independent constant. The best fit to data taken at 0.1 T leads the effective moment of 1.84 (2) μ_B, θ = -2.4 (3) K and χ_0 = 1.1 10^{-4} cm^3/mol. Fit to data taken at 14 T leads to higher effective moment of 2.59 (3) μ_B, a significantly more negative θ = -60.1 (7) K and identical temperature independent χ_0. The effective moment derived from the high field data is larger than the literature value (e.g. Ref.[17]) but it can be safely concluded that the NSC sample does not contain a sig-

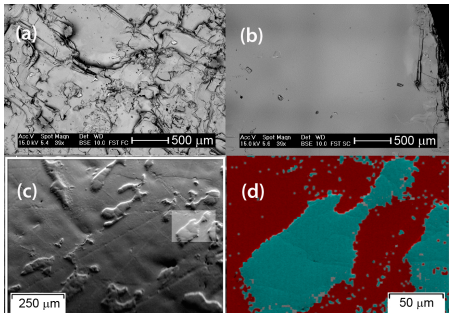

FIG. 5: (Color online) (a) SEM image obtained on the SC (inhomogeneous) sample of nominal stoichiometry $FeTe_{0.6}Se_{0.4}$ after being cleaved, demonstrating that the surface of the SC sample is highly jointed and inhomogeneous. (b) SEM image from the NSC sample of the same nominal composition after being cleaved; this crystal appears to be homogeneous. (c) SEM image obtained on the SC (inhomogeneous) sample after being cleaved and polished - inclusions are clearly visible. (d) EBSD phase distribution map of the same identical region shown in (c) (marked by a grey box) identifies the presence of different chemical compositions.

nificant amount of interstitial Fe2.

The volume character of superconductivity at 2 K within the SC sample is corroborated by a broad hysteresis loop shown for zero-field data in Fig. 4. The hysteretic magnetization curve that is typical for a superconducting material vanishes above 13 K, in agreement with the magnetic susceptibility. On the contrary, the magnetization hysteresis loop of the NSC sample shown for comparison also in Fig. 2(b) exhibits an S-shape around the origin. However, for some of the NSC samples we observe a tiny negative magnetization for the virgin initial curve. From the initial slope of both curves we derive that nearly the whole volume of the SC sample is superconducting while for the NSC sample we obtain a superconducting volume fraction of at most 1.4 %, with small variations of the superconducting volume fraction for different NSC samples. There are even samples where we do not observe superconductivity at all. This is exemplarily documented by the volume magnetic susceptibility of one of the NSC samples (see Fig. 2(b)). The magnetic susceptibility measured under field cooled (fc) and zero field cooled (zfc) conditions with the magnetic field (20 Oe) aligned along the $a-b$ plane shows a clear splitting of fc and zfc curves at 14 K. In contrast to the drop of the susceptibility at 13 K in the SC sample indicating its superconducting transition, both fc and zfc curves for the NSC sample further increase with decreasing temperature below 13 K until about 3.5 K, where a sharp peak is observed in the zfc data. This peak in zfc data appears concomitantly with a change in slope in the monotonically increasing fc data. These results are consistent with spurious superconductivity in this sample.

Nevertheless, the highly hysteretic loop recorded at 2 K on the SC sample is not only due to superconductivity in this sample. Magnetization data show that the non-homogeneous SC sample contains a phase that orders magnetically. This is documented by the magnetization hysteresis loop measured at 20 K that is shown in the inset Fig. 4, which shows also the field dependence of the magnetization measured on the NSC sample. While the NSC sample shows only an S-shaped curve without a hysteresis, the magnetization curve of the SC sample shows a complicated two-step magnetization process with a large coercitive field of 0.5 T when the field is removed. The hysteresis gets narrower with increasing temperature and eventually disappears above $\approx$ 200 K, i.e. in the temp range where the hump is observed in the susceptibility data. However, even at 300 K a small S-shape character of the magnetization curve on SC sample is still visible. On the contrary, the NSC sample exhibits no hysteresis in the whole temperature range and the S-shape character (that is present at 20 K - see the inset Fig. 4) disappears at much lower temperature of about 70-80 K. At 300 K the magnetization increases linearly with field. These findings are in accord with magnetic susceptibility measurements shown in Fig. 3 and confirm the absence of significant magnetically-ordered impurity phase (Fe, Fe_7Se_8, Fe_3Se_4 or Fe_3O_4; those materials order above room temperature and are frequently reported to be a foreign phase in the system under discussion [17,22,26]) in the NSC sample. On the other hand, the SC sample does contain a small amount of magnetically ordered phase. If normalized to the whole sample, the magnetic moment amounts to about 0.01 μ_B/Fe at 20 K.

B. Microstructure

In Figs. 5(a) and (b) we show SEM images documenting the different surface morphology of SC and NSC samples, respectively. While the surface of the former sample is highly jointed and inhomogeneous, the NSC sample is very smooth and homogenous, as expected for a single crystal of good quality. EDX performed directly on a freshly cleaved NSC sample led to composition $Fe_{1.08}Te_{0.63}Se_{0.37}$. This value is larger than that found by magnetic susceptibility and neutron diffraction data (see below). It would suggest an appreciable amount if interstitial Fe2, meaning that the sample should be indeed non-superconducting. However, it is known that EDX has somewhat reduced precission and we argue at this point that our neutron diffraction results suported by magnetic measurements indicate that the content of Fe2 in our NSC sample is well below 4 at.%. Interpretation of the EDX data of the SC sample turned out to be more difficult. While the data obtained on cleaved samples revealed slightly lower Fe content than in the case of the NSC sample, keeping the ratio between Te and Se nearly identical without significant positional dependence, further measurements on cleaved and gently polished surface revealed the existence of at least two phases (see Fig. 5(c) and Fig. 6(a)). Clearly identifiable three-dimensional inclusions with sizes of up to 250 μm

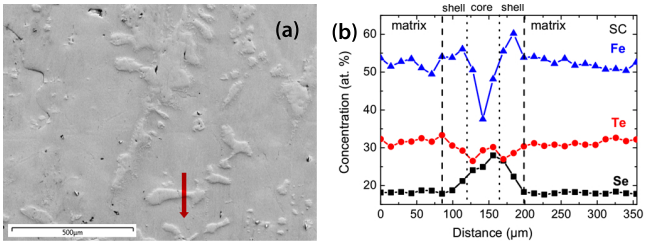

FIG. 6: (Color online) (a) Scanning electron micrograph of the inhomogeneous SC sample, revealing the presence of dendritic precipitates. (b) Linescan extracted along the arrow indicated in panel (a). The core-shell structure of the precipitates is apparent by the Fe, Se, and Te elemental distributions.

are embedded inside a matrix. The volume fraction of these inclusions can be estimated to be between 20 and 30 %.

Element distribution maps determined using the Fe-L, Se-L, and Te-L X-ray lines acquired by EDX on the area depicted in Fig. 6(a) are shown in Fig. 7(a-c). The secondary phase has a dendritic character with different compositions at the interface to the matrix with respect to the matrix and the interior of dendrits. EDX on the two phases revealed that while the matrix has average composition $Fe_{1.04}Te_{0.63}Se_{0.37}$(very similar to the NSC sample), composition of the inclusions depends on the distance from the inclusion-matrix interface. A core-shell structure of the precipitates is apparent from the positional dependence of the element compositions across the the arrow (see Fig. 6(a)) shown in Fig. 6(b). Clearly, a significant variation of the Fe and Se across the linescan is observed. While the core is strongly Fe deficient and with an excess of Se (the limiting stoichiometry is close to $Fe_{0.60}Te_{0.54}Se_{0.46}$), the shell region that is about 60 μm thick contains Fe in an excess with a gradually decreasing content of Se towards the interface with the matrix. Although the content of Te slightly varies across all the regions as well, it stays relatively constant compared to Fe and Se. Please note, that the error bars of the EDX quantification is typically of the order of 2 at.%.

The neutron diffraction data, measured on the D23 diffractometer have been corrected for anisotropic extinction and absorption using the analytical method described in refs.[33] and[34]; for simplicity the single crystal was approximated to have a rectangular shape. The corrected structure factors were fitted with the GNU XTAL SYSTEM [35] and FULLPROF[36] programs, both approaches yield comparable results. The experimental data and the best fits to them (see Table I) indicate that the NSC crystal possesses a tetragonal crystal structure (space group *P4/nmm*) with cell parameters being in good agreement with the literature[2–4]. Within this structure, the 2*a* (0, 0, 0) Wyckoff positions are occupied by iron atoms, while Se and Te share the same 2*c* (0, $\frac{1}{2}$, *z*) position, however, with different *z* parameter in agreement with the literature[4,5,26,31]. Fourier maps show that a small amount of iron (about 3.5 %, the so-called Fe2) occupies

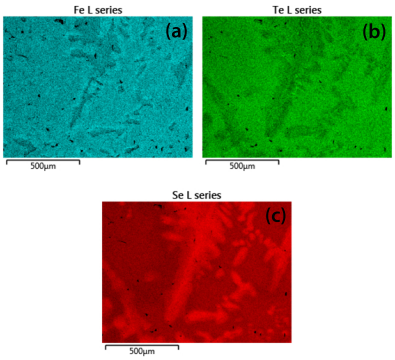

FIG. 7: (Color online) Elemental distribution maps using the (a) Fe-L, (b) Te-L, and (c) Se-L X-ray lines acquired by EDX over the same area as shown in Fig. 6(a). A core-shell structure of the precipitates is apparent.

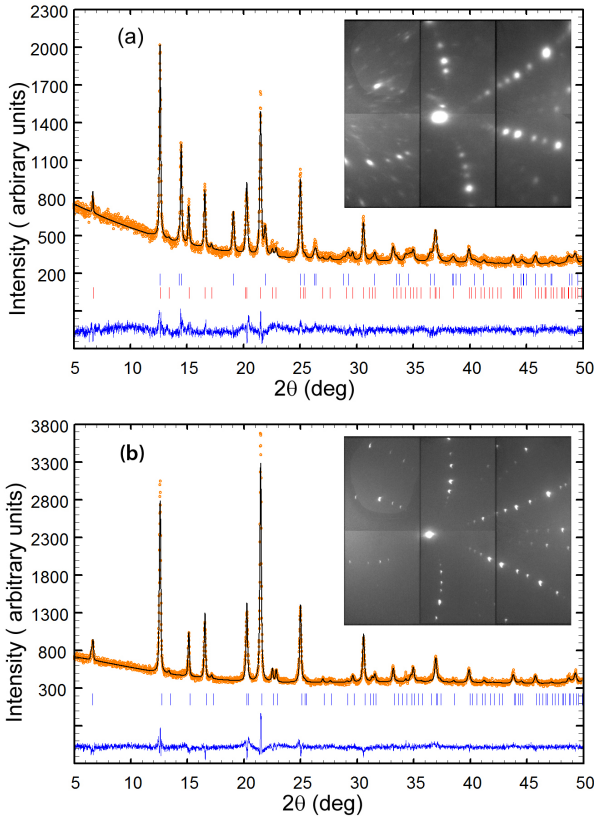

FIG. 8: (Color online) (a) X-ray powder diffractogram of the SC (inhomogeneous) sample of nominal $FeTe_{0.6}Se_{0.4}$ stoichiometry (points) together with the best fit (line through the data) and the difference (line at the bottom). The marks denote positions of the Bragg reflections belonging to the matrix (bottom row) and inclusions (top row). In the inset the neutron Laue diffractogram showing extra Bragg reflections (see the inset of (b) for comparison) is shown. In panel (b) the same is shown for the NSC (homogeneous) sample. Note the absence of the secondary phase for the NSC sample and its higher crystalline quality manifested in sharper Bragg reflections.

TABLE I: Crystal structure parameters of the NSC single crystal of the nominal composition $FeTe_{0.6}Se_{0.4}$, obtained at 1.6 K using neutron diffraction.

NSC single crystal				
Space group:	$P4/nmm$	T=1.6 K		
R_{Main}	5.0			
Cell parameter:		Occupancy:		
$a(\AA)$	3.7926(1)	Fe1	1.0(0)	
		Fe2	0.035(12)	
$b(\AA)$	3.7926(1)	Se	0.344(2)	
$c(\AA)$	6.0067(7)	Te	0.655(3)	
Atomic positions:				
Label:	site:	x	y	z
Fe1	2a	$\frac{3}{4}$	$\frac{1}{4}$	0
Se	2c	$\frac{1}{4}$	$\frac{1}{4}$	0.265(3)
Te	2c	$\frac{1}{4}$	$\frac{1}{4}$	0.274(2)
Fe2	2c	$\frac{1}{4}$	$\frac{1}{4}$	0.701(2)

TABLE II: Crystal structure parameters of the powder sample made from a NSC single crystal with nominal $FeTe_{0.6}Se_{0.4}$ composition obtained at room temperature using x-ray diffraction.

powder from NSC single crystal				
Space group:	$P4/nmm$	$T \approx 300$ K		
R_{Main}	7.7			
Cell parameter:		Occupancy:		
$a(\AA)$	3.78038(8)	Fe	1.036(0)	
$b(\AA)$	3.78038(8)	Se	0.377(6)	
$c(\AA)$	6.0475(6)	Te	0.623(5)	
Atomic positions:				
Label:	site:	x	y	z
Fe1	2a	$\frac{3}{4}$	$\frac{1}{4}$	0
Se	2c	$\frac{1}{4}$	$\frac{1}{4}$	0.2479(53)
Te	2c	$\frac{1}{4}$	$\frac{1}{4}$	0.2791(17)
Fe2	2c	-	-	-

the 2c position as well (with different z value).

Fig. 8(a) and (b) show the X-ray powder diffraction data acquired on the SC and NSC samples at room temperature. Insets show parts of neutron Laue diffractograms recorded at room temperature on single-crystalline samples along approximately the same crystallographic direction leading to very similar patterns owing to the main Bragg reflections, as expected. However, both, X-ray powder and neutron Laue diffractograms, exhibit extra Bragg reflections in the case of the SC sample. We attribute these reflections to originate from inclusions that are documented in Fig. 8(c). The X-ray diffractograms were analyzed by means of the Rietveld profile procedure using two computer codes, FULLPROF[36] and JANA2006[37]. Since $FeTe_{1-x}Se_x$ forms plate-shaped crystals with the c-axis perpendicular to the surface, a preferred orientation of the powder had to be taken into account. Also, it appeared that our X-ray data cannot be reliably used to determine the amount of Fe2. Its amount has been fixed to a values obtained either from neutron diffraction or EDX (see below).We can however, exclude any significant excess of Fe2, i.e. this result is in good agreement with structural information obtained using other methods. The best fit is shown in Fig. 8(b) by a solid line. This fit led to structural parameters (see Table II) that are in good agreement with literature. There are no unindexed reflections left in the diffractogram and the structure is described using the space group *P4/nmm*.

In Fig. 8(a), the X-ray powder diffractogram of the SC (inhomogeneous) sample together with the best fit and the difference between both is shown. The marks at the bottom denote the positions of the Bragg reflections from the matrix (bottom row) and the secondary phase (top row) that we associate with the already discussed inclusions. The symmetry of this phase is different from that of the matrix whose structure remains almost identical to the NSC sample (see structural data of Phase1 in Table III).

In the following analysis, we tested two structural models to represent the structure of the inclusions:

TABLE III: Crystal structure parameters of the powder sample made from the inhomogeneous SC single crystal with $FeTe_{0.6}Se_{0.4}$ nominal composition obtained at room temperature using x-ray diffraction.

Phase 1				
Space group:	$P4/nmm$			
R_{Main}	8.71			
Cell parameter:		Occupancy:		
$a(\AA)$	3.78319(6)	Fe	1.04(0)	
$b(\AA)$	3.78319(6)	Se	0.351(7)	
$c(\AA)$	6.0484(4)	Te	0.639(3)	
Atomic positions:				
Label:	site:	x	y	z
Fe1	2a	$\frac{3}{4}$	$\frac{1}{4}$	0
Se	2c	$\frac{1}{4}$	$\frac{1}{4}$	0.235(4)
Te	2c	$\frac{1}{4}$	$\frac{1}{4}$	0.293(1)
Fe2	2c	-	-	-
Phase 2 (core of inclusions)				
Space group:	$P6_3/mmc$			
R_{Main}	6.51			
Cell parameter:		Occupancy:		
$a(\AA)$	3.7127(2)	Fe	0.75(0)	
$b(\AA)$	3.7127(2)	Se	0.54(0)	
$c(\AA)$	5.6708(4)	Te	0.46(0)	
Atomic positions:				
Label:	site:	x	y	z
Fe	2a	0.0	0.0	0.0
Se	2c	$\frac{1}{3}$	$\frac{2}{3}$	$\frac{1}{4}$
Te	2c	$\frac{1}{3}$	$\frac{2}{3}$	$\frac{1}{4}$

(i) Since the core of inclusions have a composition close to $Fe_{0.60}Te_{0.54}Se_{0.46}$ as indicated by the EDX data, we have started with structural parameters published for monoclinic Fe_3Se_4[38]. The agreement between the best fit assuming the presence of the tetragonal matrix and monoclinic inclusions and the data is rather good. However, the refined crystal lattice parameters for the inclu-

sion phase are somewhat different as compared with stoichiometric Fe_3Se_4. This concerns mainly the monoclinic angle β, that appears to be about 90° suggesting that the actual symmetry of the lattice is higher than monoclinic. Also, the lattice constants are larger as compared to pure Fe_3Se_4, which may be assigned to the larger Te ionic radius. No correction of the preferential orientation of the secondary phase is necessary to describe the data. This is consistent with the SEM-EBSD data, which show neither a special shape nor a special mutual alignment of the inclusions with respect to the matrix.

(ii) The refined monoclinic angle β, which is very close to 90° suggests to describe the crystal structure of the inclusions by orthorhombic and hexagonal symmetry. In fact, the two descriptions are equivalent when using respective transformations and extinction rules. Assuming that the inclusions adopt a hexagonal type of structure as reported for Fe_7Se_8[39,40] we obtain a slightly better fit, while the difference to the monoclinic structure with respect to the refinement is minimal. However, we conclude that the hexagonal description is correct as the refinement of the atomic occupations (see structural data of Phase2 in Table III) leads to a stoichiometry of $Fe_{0.60}Te_{0.54}Se_{0.46}$. Another argument to favour the hexagonal description of the inclusions comes from the thermodynamic Fe-Se phase diagram where the hexagonal Fe_7Se_8 phase can easily be established in the relevant composition range[41]. The volume fraction of the secondary phase was estimated to be around 22 %, in agreement with estimates from SEM images. However, also in this case our data are not sensitive to the content of Fe2, which has been set to value found by EDX.

Although the analysis of the diffraction data may allow to assign a monoclinic structure of the inclusions, further analysis of our magnetization data are not entirely consistent since the monoclinic Fe_3Se_4 is reported to be ferrimagnetic[38,42,43] with the magnetic transition temperature and hysteretic magnetization curve even above room temperature. Our magnetization measurements are hysteretic at low temperatures but do not indicate such a behavior for the SC sample at room temperature where only an S-shape is seen. Moreover, the hysteretic magnetization curve of the SC sample has two-step character in contrast to a simple hysteresis found in Fe_7Se_8[42]. However, the magnetic properties of Fe_7Se_8 are reported to be very sensitive to iron deficiency, causing vacancies ordered within the lattice. To our knowledge, physical properties of the ternary $Fe_{0.60}Te_{0.54}Se_{0.46}$ derived from substitution of Te for Se in Fe_3Se_4 with significantly different magnetic properties (including the end-compound Fe_3Te_4) have not been studied so far. We have therefore prepared a polycrystalline sample of such a stoichiometry and checked briefly its magnetic properties. We find that the magnetic properties are roughly consistent with the "background" behavior of our SC sample.

Similar arguments apply to the hexagonal structure of the inclusions: It is known that Fe_7Se_8 orders ferrimagnetically at high temperatures and exhibits a spin-axis magnetic transition at around 130 K[44]. The fact that some groups report on the observation of magnetic transitions , e.g. at 130 K that were assigned either to the presence of Fe_3O_4 or Fe_7Se_8 may also be linked strongly to the effective cooling rates and, hence, either to oxidation or to the degree of decomposition. Fe_7Se_8 also exhibits a structural variations, depending on the preparation conditions, that differ in the way how cation vacancies are distributed[40]. Such a secondary phase, along with Fe_3O_4, has been detected in some of the previous studies[8,17–19,22,23,25,26,45–47] but was linked to the improvement of the superconductivity in inhomogeneous $FeTe_{1-x}Se_x$ only in very few of them[45–47].

The samples are also suffering from aging, i.a., the SC volume fraction increases in time and this finding is certainly related to the samples exposure to air, specifically to moisture. A very similar impact on SC when the samples were exposed to air or (hot) water was reported for e.g. $FeTe_{0.8}S_{0.2}$[48], but also for $SrFe_2As_2$[49]. Just as a side note, a similar effect is also observed when the sample is exposed to alcoholic beverages[50]. Since O_2 does not work the same way as moisture or water, some authors suggested that the presence of H^+ and its intercalation is responsible for the observed SC. However, as alternative scenario and in particular in the light of our results, one may conclude that the presence of moisture triggers in spurious parts of the sample the phase formation from the NSC tetragonal material to the SC material. Such aging or decomposition effects may contribute to the observation of the minute (up to 1 vol.%) and slightly varying amount of SC in different NSC samples.

III. DISCUSSION AND CONCLUSIONS

Our study have shown that two single-crystalline samples with the identical starting stoichiometry of $FeTe_{1-x}Se_x$ show significantly different microstructure, magnetic and electrical transport properties depending on the cooling rate. It appears that the sample cooled down slowly (thermodynamic control of the phase composition) is homogeneous and of much better single-crystalline quality. This is documented by sharper neutron-Laue Bragg reflections as seen in insets of Fig. 8(a) and (b) and suggests stress-free conditions in this non-superconducting sample. The crystal structure is of tetragonal PbO-type. On the contrary, the superconducting sample shows much broader Bragg reflections.

The EDX and neutron diffraction results show that this sample is nearly stoichiometric with slight Fe excess not larger than $\approx$ 4 %. The fastly cooled sample composition determined by kinetic control is heterogeneous, containing from a matrix (about 70 % of the volume) and inclusions. The matrix has the same crystal structure as the homogeneous sample. The composition of the matrix is within error bars also the same. One can thus conclude that high crystalline quality and purity is not favourable

for the occurence of superconductivity in this system. It is also not the amount of the interstitial Fe2 that trigers the superconductivity in one sample but prohibits it in the other one.

The secondary phase found in the SC sample precipitates in a form of a three-dimensional network of inclusions. These inclusions that are most probably hexagonal consist from two regions: a core with composition close to $Fe_{0.60}Te_{0.54}Se_{0.46}$ and shell regions between the core and the matrix that contain excess of Fe and strongly varying Se. The amount of the secondary phase does not allow to conclude whether it percolates through the sample. Nevertheless, one can safely exclude that the core region is itself superconducting as it can be identified as magnetically ordered Fe_3Se_4 -related material. Another situation applies for the shell region that contains excess of Fe. These regions might percolate through the sample. However, it is not very plausibel that this phase superconducts as it is generally accepted that the excess of iron is anthagonistic with superconductivity. What remains is the matrix itself. However, the matrix of both samples are from the chemical point of view not distinguishable. The difference lies in their crystallographic quality, the SC sample being by far less perfect. This could be, for instance caused by a spread of lattice constants as a result of (i) compositional fluctuations or (ii) presence of stresses in the sample.

As we do not observe significant variation of the composition of the matrix (that one observed would not cause such a large spread of lattice constants), we concentrate on the second scenario. Interesting point in this respect is that while Fe_3Se_4 is reported to adopt either monoclinic or hexagonal structure[45], the Fe_7Se_8 crystallizes in either triclinic or hexagonal type (however, the lattice constants are not compatible with by us determined secondary phase lattice constants due to presence of Te) of structure and the Fe_3O_4 is cubic, the identified secondary phase adopts the hexagonal symmetry. Lattice constants are very close to those of NiAs-type FeSe that is found to be superconducting below 8 K[1]. This value is much lower that observed 13 K. It is well known that the application of pressure on FeSe increases $T-sc$ from 8.5 K up to $\approx$ 37 K[9]. Interestingly, the originally tetragonal structure is gradually transformed to a hexagonal NiAs-type lattice, with both structures coexiisting in a wide range of pressures. Even more interesting is the fact that the maximal $T-sc$ value is attained at region where the hexagonal type of structure commences to appear. Therefore it is tempting to conclude that the superconductivity appears in the SC sample either (i) within the shell regions of the hexagonal secondary phase that percolatse the sample or (ii) within the tetragonal matrix that is subjected to internal stress at the interface regions.

Although we could not unambiguously identify the superconducting phase, we conclude that the presence of different crystallographic phases (here notably the presence of the hexagonal phase) is the key ingredient responsible for the occurrence of the superconductivity in this system. These conclusions are in agreement with studies of Wittlin *et al.*[45]. The magnetic contribution of the core regions of the secondary phase seems to be in this light merely a complication that obscurs the interpretation of experimental values (in contrary to the destructive influence of the interstitial Fe2). In any case, we can exclude that the freshly prepared, slowly-cooled homogeneous $FeTe_{0.6}Se_{0.4}$ system in the absence of any secondary phase would be superconducting in its stress-free state. Whether the superconductivity in the NSC system can be induced by stress is yet to be tested.

Acknowledgments

We acknowledge greatly the ILL Grenoble for the allocated beamtime and Christiane Förster from HZB for preparation of samples for EDX and fruitful discussion of the results. S.W. gratefully acknowledges funding by Deutsche Forschungsgemeinschaft DFG in project WU 595/3-1 (Emmy Noether programme). This project was funded by DFG in SPP1458 (projects BU887/15-1 and AR613/12) and by Bundesministerium für Bildung und Forschung (BMBF) in the ERA.Net RUS program (project #245 FeSuCo). We thank Th. Wolf and A. Maljuk for valuable discussion, L. Giebeler for support with XRD data acquisition and M. Reehuis for help with using GNU Xtal system.

* Electronic address: prokes@helmholtz-berlin.de
† Electronic address: s.wurmehl@ifw-dresden.de

[1] F.-C. Hsu, J.-Y. Luo, K.-W. Yeh T.-K. Chen, T.-W. Huang, P. M. Wu, Y.-C. Lee, Y.-L. Huang, Y.-Y. Chu, D.-C. Yan and M.-K. Wu, Proc. Nat Acad. Sci. USA **105**, 14262 (2008).
[2] K. Horigane, H. Hiraka and K. Ohoyama, J. Phys. Soc. Jpn., **78**, 074718 (2009).
[3] M.C. Lehman, A. Llobet, K. Horigane and D. Louca, Journal of Physics: Conf. Ser., **251**, 012009 (2010)
[4] M. Tegel, C. Löhnert and D. Johrendt, Solid State Comm., **150**, 383 (2010).
[5] Y. Miziguchi and Y. Takano, J. Phys. Soc. Jpn., **79**, 102001 (2010).
[6] T. J. Liu, J. Hu, B. Qian, D. Fobes, Z. Q. Mao, W. Bao, M. Reehuis, S. A. J. Kimber, K. Prokeš, S. Mat'aš, D. N. Argyriou, A. Hiess, A. Rotaru, H. Pham, L. Spinu, Y. Qiu, V. Thampy, A. T. Savici, J. A. Rodriguez and C. Broholm, Nature Materials **9**, 716 (2010).
[7] K.W. Yeh, H.C. Hsu, T.W. Huang, P.M. Wu, Y.L. Huang, T.K. Chen, J.Y. Luo and M.K. Wu, J. Phys. Soc. Jpn., Suppl. C., **77**, 19 (2008).

[8] G. R. Stewart, Reviews of Modern Physics **83**, 1589 (2011).
[9] S. Medvedev, T. M. McQueen, I. A. Troyan, T. Palasyuk, M. I. Eremets, R. J. Cava, S. Naghavi, F. Casper, V. Ksenofontov, G. Wortmann and C. Felser, Nature Materials **8**, 630 (2009).
[10] K. Miyoshi, K. Morishita, E. Mutou, M. Kondo, O. Seida, K. Fujiwara, J. Takeuchi and S. Nishigori, J. Phys. Soc. Jpn., **83**, 013702 (2014)
[11] W. Bao, Y. Qiu, Q. Huang, M. A. Green, P. Zajdel, M. R. Fitzsimmons, M. Zhernenkov, S. Chang, M. Fang, B. Qian, E. K. Vehstedt, J. Yang, H. M. Pham, L. Spinu and Z. Q. Mao, Phys. Rev. Lett. **102**, 247001 (2009).
[12] D. C. Johnston Advances in Physics **59**, 803 (2010).
[13] M. H. Fang, H. M. Pham, B. Qian, T. J. Liu, E. K. Vehstedt, Y. Liu, L. Spinu, and Z. Q. Mao, Phys. Rev. B **78**, 224503 (2008).
[14] N. Katayama, S. Ji, D. Louca, S. Lee, M. Fujita, T. J. Sato, J. Wen, Z. Xu, G. Gu, G. XU, Z. Lin, M. Enoki, S. Chang, K. Yamada and J. M. Tranquada, J. Phys. Soc. Jpn., **79**, 113702 (2010)
[15] R. Khasanov, M. Bendele, A. Amato, P. Babkevich, A. T. Boothroyd, A. Cervellino, K. Conder,. N. Gvasaliya, H. Keller, H.-H. Klauss, H. Luetkens, V. Pomjakushin, E. Pomjakushina, and B. Roessli, Phys. Rev. B **80**, 140511(R) (2009).
[16] M. Bendele, P. Babkevich, S. Katrych, S. N. Gvasaliya, E. Pomjakushina, K. Conder, B. Roessli, A. T. Boothroyd, R. Khasanov, and H. Keller, Phys. Rev. B **82**, 212504 (2010).
[17] S. Rößler, D. Cherian, S. Harikrishnan, H. L. Bhat, S. Elizabeth, J. A. Mydosh, L. H. Tjeng, F. Steglich,and S. Wirth, Phys. Rev. B **82**, 144523 (2010).
[18] J. Yang, M. Matsui, M. Kawa, H. Ohta, Ch. Michioka, Ch. Dong, H. Wang, H. Yuan, M. Fang, and K. Yoshimura, J. Phys. Soc. Jpn., **79**, 074704 (2010).
[19] R. Viennois, E. Giannini, D. van der Marel, and R. Černý, J. Solid State Chem. **183** 769 (2010).
[20] T. J. Liu, X. Ke, B. Qian, J. Hu, D. Fobes, E. K. Vehstedt, H. Pham, J. H. Yang, M. H. Fang, L. Spinu, P. Schiffer, Y. Liu, and Z. Q. Mao, Phys. Rev. B **80**, 147509 (2009).
[21] W. Bao, Y. Qiu, Q. Huang, A. Green, P. Zajdel, M. R. Fitzsimmons, M. Zhernenkov, M. Fang, B. Qian, E. K. Vehstedt, J. Yang, H. M. Pham, L. Spinu, and Z. Q. Mao: Phys. Rev. Lett. **102** (2009) 247001.
[22] V. Tsurkan, J. Deisenhofer, A. Günther, Ch. Kant, M. Klemm, H.-A. Krug von Nidda, F. Schrettle and A. Loidl, Eur. Phys. J. B **79**, 289 (2011).
[23] T. Taen, Y. Tsuchiya, Y. Nakajima, and T. Tamegai, Phys. Rev. B **80**, 092502 (2009).
[24] T. Noji, T. Suzuki, H. Abe, T. Adachi, M. Kato, and Y. Koike, J. Phys. Soc. Jpn., **79**, 084711 (2010).
[25] J. Wen, G. Xu, G. Gu, J. M. Tranquada, and R. J. Birgeneau, Rep. Prog. Phys. **74**, 124503 (2011).
[26] M. Bendele, S. Weyeneth, R. Puzniak, A. Maisuradze, E. Pomjakushina, K. Conder, V. Pomjakushin, H. Luetkens, S. Katrych, A. Wisniewski, R. Khasanov and H. Keller, Phys. Rev. B **81**, 224520 (2010).
[27] Y. Mizuguchi, F. Tomioka, S. Tsuda, T. Yamaguchi, Y. Takano, J. Phys. Soc. Jpn., **78**, 074712 (2009).
[28] B. C. Sales, A. S. Sefat, M. A. McGuire, R. Y. Jin, D. Mandrus and Y. Mozharivskyj, Phys. Rev. B **79**, 094521 (2009).
[29] X. He, G. Li, J. Zhang, A. B. Karki, R. Jin, B. C. Sales, A. S. Sefat, M. A. McGuire, D. Mandrus, and E. W. Plummer, Phys. Rev. B **83**, 220502(R) (2011).
[30] A. Iadecola, B. Joseph, L. Simonelli, Y. Mizuguchi, Y. Takano and N. L. Saini, Euro. Phys. Lett. **90**, 67008 (2010).
[31] B. Joseph, A. Iadecola, A. Puri, L. Simonelli, Y. Mizuguchi, Y. Takano and N. L. Saini, Phys. Rev. B **82**, 020502(R) (2010).
[32] N. R. Werthamer, E. Helfand, P. C. Hohenberg, Phys. Rev. **147** 295 (1966).
[33] J. de Meulenaer and H. Tompa, Acta Cryst. **19**, 1014 (1965).
[34] N. Alcock, Acta Cryst. **30**, 332 (1973).
[35] S. R. Hall, D. J. du Boulay, and R. Olthof-Hazekamp, Xtal3.7 System University of Western Australia (2000).
[36] T. Roisnel and J.Rodrguez-Carvajal, Materials Science Forum **378**, 118 (2001).
[37] V. Petríček, M. Dušek, and L. Palatinus, Jana2006. The crystallographic computing system. Institute of Physics, Praha, Czech Republic (2006).
[38] A. F. Andresen, Acta Chemica Scandinavia, **22**, 827 (1968).
[39] A. Okazaki, K. Hirakawa, J. Phys. Soc. Jpn. **11**, 930 (1956).
[40] A. Okazaki, J. Phys. Soc. Jpn., **16**, 1162 (1961).
[41] H. Okamoto, J. Phase Equilib., **12**, 383 (1991).
[42] J. Wang, H. Duan, X. Lin, V. Aguilar, A. Mosqueda and G.-M. Zhao, J. Appl. Phys., **112**, 103905 (2012).
[43] G. Long, H. Zhang, D. Li, R. Sabirianov, Z. Zhang and H. Zeng, Appl. Phys. Lett., **99**, 202103 (2011).
[44] T. Takahashi, J. Phys. Soc. Jpn., **43**, 1594 (1977).
[45] A. Wittlin, P. Aleshkevych, H. Przybylińska, D. J. Gawryluk, P. Dłużewski, M. Berkowski, R. Puźniak, M. U. Gutowska and A. Wiśniewski, Supercond. Sci. Technol. **25**, 065019 (2012).
[46] H. Hu, J.-M. Zuo, J. Wen, Z. Xu, Z. Lin, Q. Li, G. Gu, W. K. Park, L. H. Greene, New Journal of Physics **13**, 053031 (2011).
[47] V. Bhatia, E. E. Rodriguez, N. P. Butch, J. Paglionec, M. A. Green, Chem. Commun., **47**, 11297 (2011).
[48] Y. Mizuguchi, K. Deguchi, S. Tsuda, T. Yamaguchi and Y. Takano, *Phys. Rev. B* **81**, 214510 (2010).
[49] H. Hiramatsu, T. Katase, T. Kamiya, M. Hirano and H. Hosono, *Phys. Rev. B* **80**, 052501 (2009).
[50] K. Deguchi, Y. Mizuguchi, T. Ozaki, S. Tsuda, T. Yamaguchi and Y. Takano, *Supercond. Sci. Technol.* **24**, 055008 (2011)